Journal of Process Control 129 (2023) 103033

Contents lists available at ScienceDirect

Journal of Process Control

journal homepage: www.elsevier.com/locate/jprocont

Extremum seeking control to optimize mineral recovery of a flotation circuit using peak air recovery

D.A. Wepener, J.D. le Roux *, I.K. Craig

Department of Electrical, Electronic and Computer Engineering, University of Pretoria, Pretoria, South Africa

ARTICLE INFO

Article history:
Received 19 October 2022
Received in revised form 22 June 2023
Accepted 5 July 2023
Available online 24 July 2023

Keywords:
Extremum seeking control
Flotation circuit
Peak air recovery
Process control
Optimization

ABSTRACT

A flotation circuit is controlled in simulation using an extremum seeking control (ESC) approach to keep the cells operating at the optimal operating point, as represented by peak air recovery. It is assumed that optimal performance is achieved at this operating point where the froth layer is stable, and the mineral recovery of the flotation cell is maximized. Two gradient-based ESCs, a classical perturbation-based ESC and a time-varying ESC, as well as a non-gradient-based direct search Nelder–Mead simplex ESC, are compared on the flotation circuit to steer the plant through an unknown static map towards the peak in air recovery. The three ESCs can respectively optimize the flotation circuit and find the peak air recovery operating point. The simplex ESC can converge quickly to the optimum but does not adapt to changing conditions. The gradient-based ESCs can track the time-varying peak air recovery operating point and adapt to an external disturbance. Although the three ESC methods are not dependent on a process model to optimize the plant, their convergence times are relatively slow. The ESCs are ideally suited for model-independent long-term automated optimization of a flotation circuit with a slow time-varying optimal operating point.

© 2023 The Author(s). Published by Elsevier Ltd. This is an open access article under the CC BY-NC-ND license (http://creativecommons.org/licenses/by-nc-nd/4.0/).

1. Introduction

Flotation is a separation process that concentrates minerals by using the hydrophobicity properties of the minerals. A flotation cell is used to separate the hydrophobic particles from the hydrophilic particles in a three-phase system [1]. The three phases refer to the mineral particles (solid), water (liquid) and air (gas) that interacts with each other inside a flotation cell. The aim of the flotation process is for the valuable mineral particles to attach to air bubbles introduced in the flotation tank and flow to the top of the tank while the gangue flows to the bottom. In the industry, flotation cells are connected in flotation banks, and each bank has a specific function in the flotation process. The functions of the flotations banks can be divided into three sections: rougher, scavenger and cleaner banks [2].

The success of a flotation process depends on two main performance indicators: mineral recovery and product grade. The recovery is the fraction of the total amount of valuable minerals in the feed that are concentrated, and the grade is the ratio of valuable minerals to gangue in the final product. The control objective of each flotation cell is to maximize grade and recovery, but there is an inverse relationship between grade and recovery [2,3]. Flotation is a complicated process with many interacting variables that makes the process difficult to model accurately. Without an accurate model, advanced process control for flotation optimization becomes challenging to implement and less effective [4].

In the mineral processing industry, there is an incentive for improved optimization control, especially long-term automated advanced optimization [5–7]. One possible solution for optimization control of a flotation circuit is peak air recovery. Hadler and Cilliers [8] report that the optimal performance of a flotation cell can be found by maximizing the air recovery of the cell and operating at the peak air recovery point. The froth is stabilized at this optimal operating point, and the mineral recovery is maximized while the grade is kept at an acceptable level [9].

The use of peak air recovery as an optimization objective differs from typical optimization approaches such as mass pull control, the direct control of grade and recovery, or economic control by optimizing the net smelter return. Using two case studies, Hadler et al. [9] demonstrated that an increase in mass pull does not necessarily yield an increase in mineral recovery. Rather, there is a potential for improved performance when operating at peak air recovery conditions. Peak air recovery optimization can also be advantageous over grade and recovery or economic controllers as it is only dependent on a single measurement of air recovery that can be obtained from a vision-based system and does not require any elemental assays. An impediment to using peak air recovery for optimization control is that the peak is time-varying, and the required aeration rate that results in

* Corresponding author.
E-mail address: derik.leroux@up.ac.za (J.D. le Roux).

https://doi.org/10.1016/j.jprocont.2023.103033
0959-1524/© 2023 The Author(s). Published by Elsevier Ltd. This is an open access article under the CC BY-NC-ND license (http://creativecommons.org/licenses/by-nc-nd/4.0/).

peak air recovery continuously shifts [10]. The fluctuation in air recovery may be due to changing ore characteristics or upstream conditions that propagate to the flotation circuit [11]. This makes it difficult to operate the flotation plant optimally at all times. The solution proposed in this article is to use extremum seeking control (ESC) to maximize the air recovery and keep the flotation cell operating at the time-varying peak air recovery.

ESC is an optimization technique that maximizes an objective function by exploring an unknown static map and steering the system towards the optimal operating condition [12,13]. ESC is a model-free adaptive controller and does not use any explicit knowledge of the process dynamics. This is an advantage for flotation control due to the challenges of accurately modeling the process. However, ESC has some drawbacks, the most important being the slow convergence time to the optimum compared to model-based adaptive controllers [14]. ESC is best suited in the optimization layer of a control framework, operating on top of the supervisory and regulatory control layers to steer a process variable such as air recovery to the optimum. Therefore, ESC is ideally suited to track and maintain peak air recovery for a flotation cell.

This work expands on Wepener et al. [15] and describes the first application of ESC to a flotation circuit. In particular, a newly developed flotation circuit model [16], verified on industrial data, is used to illustrate the feasibility of applying ESC to flotation and the impact that it may have on optimizing the process. Continuously maximizing the air recovery in a flotation cell can be achieved with an ESC by directly manipulating the aeration rate to the cell leading to increased recovery of the flotation circuit. This paper explores three different ESC methods: two gradient-based methods (a perturbation-based and a time-varying method), and a non-gradient-based Nelder–Mead simplex method.

The flotation process is described in Section 2, the process model description is given in Section 3, and air recovery is discussed in Section 4. In Section 5, an overview is given of the three ESCs that are investigated, and in Section 6, the simulation setup is presented. The results are presented and discussed in Section 7, and the work is concluded in Section 8 by discussing the advantages and shortcomings of the ESCs.

2. Process description

The mineral processing chain consists of two main stages: the comminution stage and the separation stage. The run-of-mine ore first passes through the comminution stage, most often a grinding circuit, where the ore is ground into fine particles and mixed with water to form a slurry. The slurry then flows to the separation stage, where the valuable minerals are separated from the gangue. There are many types of separation circuits, but this study will focus only on flotation. In industry, flotation tanks are connected in flotation banks, with each bank performing a specific function. The functions of the flotations banks can usually be divided into three sections: rougher, scavenger and cleaner banks [2]. The flotation circuit used in this simulation study includes four flotation cells in the rougher section. The four cells are connected in series, as shown in Fig. 1.

The slurry from the comminution stage flows into the first flotation cell with a flow rate, Q_{F_1}. The tailings flow rates of the slurry flowing out of the cells are given by Q_{T_k}, where k is the cell number. The aeration rate to each cell, Q_{Air_k}, gives the flow rate of air flowing into the cell, forming bubbles that rise through the slurry. The measurement of the aeration rate is the superficial gas velocity. As the air bubbles rise, the valuable mineral particles attach to the bubbles because of their hydrophobicity and collect in the froth layer at the top of the cell. The froth height is denoted by h_{f_k} while L_k is the pulp level in each cell. The air bubbles in the froth layer flow over the cell lip into the concentrate launder with flow rates, Q_{C_k}, and collect in the concentrate hopper. The slurry level in the hopper is given by L_H. The concentrate is pumped away from the hopper for further processing with a flow rate of Q_H.

3. Model description

The dynamic model of a four-cell flotation circuit, as shown in Fig. 1 and given in [16], is used to simulate the performance of the proposed controller. Each of the flotation cells has the following states, the cell pulp level (L_k), the masses in the cell ($M_k^{i,j}$), the air recovery (α_k) and the top of froth bubble size (D_{BF_k}). The superscript, i, represents the different mineral species in the cell (gangue or valuable minerals), and j represents the different sub-classes within the mineral class for minerals with different flotabilities or sizes. This simulation study simplifies the model to include only two mineral species, valuable minerals ($i = 0$) and gangue ($i = 1$). It is also assumed that there are no sub-classes, and j will therefore be omitted. A comprehensive model description can be found in [16].

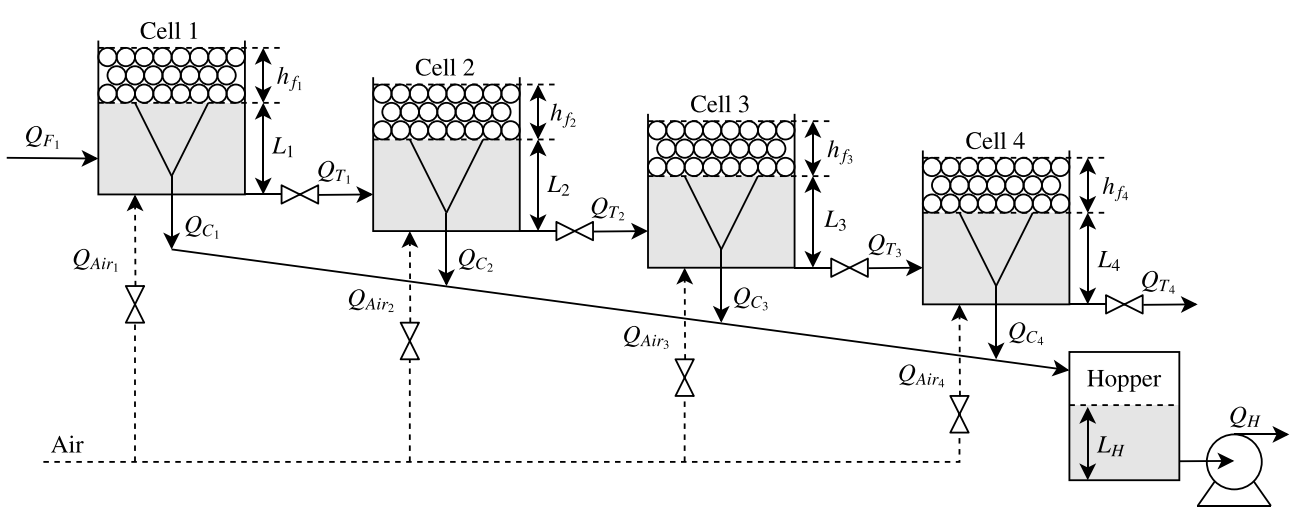

Fig. 1. Flotation circuit configuration.
Source: Adapted from [16].

Table 1
Description of flotation model variables.

Variable	Unit	Description
i	–	Superscript for mineral species: valuable mineral ($i = 0$) and gangue ($i = 1$)
$k,\ H$	–	Subscript for unit (flotation cell k, or hopper, H)
$\square$	–	Subscripts for feed ($\square = F$), tails ($\square = T$), concentrate ($\square = C$)
$A_k,\ A_H$	m^2	Surface area of cell k or hopper H
h_k	m	Difference in height between cell k and $k+1$
ρ_s^i	kg/m^3	Density of mineral species i
λ_{out}	–	Plateau border length per volume of froth
K^i	–	Pseudo rate-constant of mineral species i
λ_{air_k}	s	Average froth residence time in cell k
S_{b_k}	s^{-1}	Bubble surface area flux in cell k
Ent^i_{Frac}	–	Entrainment factor of mineral species i
$Q_{\square_k},\ Q_H$	m^3/h	Volumetric flow rate associated with cell k or hopper H
Q_{air_k}	m^3/h	Volumetric air flow rate to cell k
$\dot{M}^i_{\square_k}$	kg/h	Mass flow rate of mineral species i associated with cell k
C_{v_k}	$m^{5/2}/h$	Valve constant for cell k
v_k	–	Valve position for cell k
h_{f_k}	mm	Froth depth of cell k
J_{g_k}	mm/s	Superficial gas velocity for cell k
J_{gSP_k}	mm/s	Superficial gas velocity setpoint for cell k
$\tau_{J_{g_k}}$	s	First order time constant of the air valve response of cell k

The change in the pulp level of each cell is modeled using the volume balance in the cell,

$$\frac{d}{dt}L_k = \frac{Q_{F_k} - Q_{T_k} - Q_{C_k}}{A_k}, \tag{1}$$

where A_k is the surface area of cell k. The effect of a change in gas holdup on the change in level is not included in the model as it is relatively small compared to the effect of the flow rates, and it changes on a much slower time scale. The tailings flow rate from the cell (Q_{T_k}) is the feed flow rate into the next cell ($Q_{F_{k+1}}$) and is modeled according to [17],

$$Q_{T_k} = C_{v_k} v_k \sqrt{L_k - L_{k+1} + h_k}, \tag{2}$$

where C_{v_k} is the valve constant for valve position, v_k, and h_k is the physical difference in height between the two cells. A mass balance is used to model the change in mass in each cell,

$$\frac{d}{dt}M^i_k = \dot{M}^i_{F_k} - \dot{M}^i_{T_k} - \dot{M}^i_{C_k}, \tag{3}$$

where $\dot{M}^i_{\square_k}$ is the mass flow rate associated with the feed ($\square = F$), tailings ($\square = T$) or concentrate ($\square = C$) of cell k. The tailings mass flow rate of cell k is the feed flow rate of the next cell, $\dot{M}^i_{F_{k+1}} = \dot{M}^i_{T_k}$, and is calculated by,

$$\dot{M}^i_{T_k} = \frac{M^i_k}{L_k A_k} Q_{T_k}. \tag{4}$$

The concentrate mass flow rate includes true flotation and entrainment components. True flotation occurs when a particle collides with a bubble, attaches to its surface and rises to the froth. Entrainment occurs when the particle is dragged to the froth by the liquid between the bubbles. The concentrate mass flow rate is given by,

$$\dot{M}^i_{C_k} = K^i M^i_k S_{b_k} \alpha_k + Ent^i_{Frac} \frac{M^i_k}{A_k L_k} Q_{C_k}, \tag{5}$$

where K^i is a pseudo rate-constant, M^i_k is the mass of mineral i in cell k, S_{b_k} is the bubble surface area flux, α_k is the air recovery (see (9)), and Ent^i_{Frac} is the entrainment factor. The concentrate flow rate is calculated from water recovery and true flotation models,

Table 2
Description of flotation model states.

Variable	Unit	Description
$L_k,\ L_H$	m	Pulp level in cell k or hopper H
$M^i_k,\ M^i_H$	kg	Masses of mineral species i in cell k or hopper H
α_k	–	Air recovery in cell k
D_{BF_k}	mm	Top of froth bubble diameter in cell k

$$\frac{Q_{C_k}}{A_k} = \begin{cases} \dfrac{J^2_{g_k}\lambda_{out}}{k_1}(1-\alpha_k)\alpha_k + \dfrac{d}{dt}M^i_{TF_k}/\rho^i_s & 0 < \alpha_k < 0.5 \\ \dfrac{J^2_{g_k}\lambda_{out}}{4k_1} + \dfrac{d}{dt}M^i_{TF_k}/\rho^i_s & \alpha_k \geq 0.5 \end{cases}, \tag{6}$$

where $\frac{d}{dt}M^i_{TF_k} = K^i M^i_k S_{b_k}\alpha_k$ is the mass flow rate of mineral i to the froth phase in cell k due to true flotation, and ρ^i_s is the density of the mineral. J_{g_k} is the superficial gas velocity for cell k, and k_1 is a constant. The superficial gas velocity is linearly related to the aeration rate,

$$J_{g_k} = 3.6\frac{Q_{Air_k}}{A_k}. \tag{7}$$

The Plateau border length (λ_{out}) per volume of froth is inversely proportional to the square of the top of froth bubble diameter (D_{BF_k}),

$$\lambda_{out} \approx \frac{6.81}{D^2_{BF_k}}. \tag{8}$$

The models for air recovery and the bubble size are empirical models derived by [16] using industrial data. The change in air recovery is,

$$\frac{d}{dt}\alpha_k = \frac{\alpha_{SS_k} - \alpha_k}{\lambda_{air_k}}, \tag{9}$$

where λ_{air_k} is the average froth residence time,

$$\lambda_{air_k} = \frac{h_{f_k}}{J_{g_k}}. \tag{10}$$

The steady-state model of air recovery, α_{SS_k}, is given by,

$$\alpha_{SS_k} = K_{\alpha_{J_g}}\left(J_{g_k} - K_{\alpha_{J_{gk}}} - K_{\alpha_{h_f}} h_{f_k}\right)^2 + \alpha_{OS_k}. \tag{11}$$

Table 3
Description of flotation model empirical parameters.

Variable	Description
α_{SS_k}	Steady-state value of air recovery in cell k
$K_{\alpha_{J_{gk}}}$	Value of the superficial gas velocity in cell k where air recovery is maximized when $h_{f_k} = 0$
$K_{\alpha_{J_g}}$	Effect of the difference between J_{g_k} and $K_{\alpha_{J_{gk}}}$ squared on air recovery
$K_{\alpha_{h_f}}$	Effect of a change in h_{f_k} on the superficial gas velocity where air recovery is maximized
α_{OS_k}	Offset included in steady-state air recovery in cell k
$K_{BF_{J_g}}$	Effect of the superficial gas velocity on the mean top-of-froth bubble diameter
K_{BF_λ}	Effect of the average froth residence time on the mean top-of-froth bubble diameter
D_{OS_k}	Offset included in steady-state top-of-froth bubble diameter in cell k

The parameters, $K_{\alpha_{J_g}}$, $K_{\alpha_{J_{gk}}}$, $K_{\alpha_{h_f}}$ and α_{OS_k} are empirically fitted. $K_{\alpha_{J_g}}$ is a negative constant to create a parabolic shape in the air recovery as a function of the aeration rate. The parabola has a peak in air recovery where $J_{g_k} = K_{\alpha_{J_{gk}}} + K_{\alpha_{h_f}} K_{\alpha_{h_f}}$. The rate of change in bubble size is,

$$\frac{d}{dt} D_{BF_k} = \frac{K_{BF_{J_g}} J_{g_k} + K_{BF_\lambda} \lambda_{air_k} - D_{OS_k}}{\lambda_{air_k}}, \tag{12}$$

where $K_{BF_{J_g}}$, K_{BF_λ} and D_{OS_k} are empirically fitted parameters. The dynamic responses of superficial gas velocities (J_{g_k}) to setpoint changes (J_{gSP_k}) are defined with first-order models with unity gains,

$$\frac{d}{dt} J_{g_k} = \frac{J_{gSP_k} - J_{g_k}}{\tau_{J_{g_k}}}, \tag{13}$$

where $\tau_{J_{g_k}}$ is the first order time constant of the air valve response of cell k. The concentrate hopper has two states, the hopper level (L_H) and the masses in the hopper (M_H^i). The state equations are,

$$\frac{d}{dt} L_H = \frac{Q_{C_1} + Q_{C_2} + Q_{C_3} + Q_{C_4} - Q_H}{A_k}, \tag{14}$$

$$\frac{d}{dt} M_H^i = \sum_{k=1}^{4} \dot{M}_{C_k}^i - \frac{M_H^i}{L_H A_H} Q_H. \tag{15}$$

The total mass pull rate of the hopper is given by,

$$\dot{M}_H^{Tot} = \left(\dot{M}_H^0 + \dot{M}_H^1\right) \frac{Q_H}{L_H A_H}. \tag{16}$$

The concentrate grade in the hopper is the ratio of the desired mass to the total mass in the hopper,

$$\text{Grade} = \frac{M_H^0}{M_H^0 + M_H^1}. \tag{17}$$

An *instantaneous* mineral recovery is given by,

$$\text{Recovery} = \frac{\sum_{k=1}^{4} \dot{M}_{C_k}^0}{\dot{M}_{F_1}^0}, \tag{18}$$

where $\dot{M}_{C_k}^0$ is the desired element mass flow rate in the concentrate stream of cell k and $\dot{M}_{F_1}^0$ is the desired element mass flow rate in the feed stream. Although recovery is generally calculated at steady-state, the *instantaneous* recovery is a useful real-time approximation.

The variables used in the flotation model are summarized in Table 1, and the model states are given in Table 2. Table 3 shows all the empirical parameters to be estimated. The nominal values of the variables, states and estimated empirical parameters are taken from Oosthuizen et al. [16].

4. Air recovery

Air recovery is the fraction of the air that enters the flotation cell and overflows the lip of the cell inside unburst bubbles. Air recovery can be seen as a measure of the stability of the froth in the flotation cell. Therefore, it is an indicator that can be used to evaluate the efficiency and performance of the flotation process. The equation for air recovery is given by [9],

$$\alpha = \frac{v_f \cdot h \cdot w}{Q_{Air}}, \tag{19}$$

where v_f is the overflow velocity of the froth, h is the overflow froth height above the cell lip, w is the overflow length, and Q_{Air} is the inlet air flow rate. In industrial flotation plants, the air recovery can be measured with a froth vision system, and laser-based froth height measurement [10,18]. For the simulation study, a simplified air recovery model is used as given in (9)–(11) in Section 3.

Fig. 2 shows the steady-state simulation of air recovery for different aeration rates and froth heights using the model described in Section 3. Although the surfaces for an industrial plant would contain more noise and would be time-varying, the general parabolic shape remains [7–10]. Air recovery initially increases with an increase in the aeration rate, but it reaches a peak, after which a further increase in the aeration rate lowers the air recovery. At a low aeration rate, the bubbles rise slowly through the slurry to produce highly laden, well-drained froths. The bubbles often collapse before overflowing the cell lip. The low aeration rate results in a high concentrate grade but with low air recoveries and low mineral recoveries. At a high aeration rate, past the air recovery peak, the air moves fast through the cell, creating unstable bubbles that burst before they reach the top. These bubbles have a higher water content as the water becomes trapped between the bubbles, which reduces the grade.

The steady-state model simulations of the mineral recovery and grade, measured in the concentrate hopper, shown in Fig. 2, show the inverse relationship between grade and recovery. The aeration rates that create the peaks on the recovery curve also correspond approximately to the low points on the grade curve.

The froth height (h_{f_k}) has a much smaller effect on the air recovery than the aeration rate, and the plant is able to reach the peak air recovery operating point at any froth height by changing the aeration rate. When controlling for air recovery only, the benefits of controlling the froth height as well as the aeration rate do not outweigh the disadvantages that come with the added complexity of implementing a multiple-input controller and the possibility of reduced froth stability. Throughout the rest of the study, the froth heights were kept constant at a setpoint, and only the aeration rate was varied. Fig. 3 shows the effect of the aeration rate on the air recovery, grade and recovery while the froth height is kept constant at a setpoint.

5. Extremum seeking control

ESC is a control approach that is used to optimize a system by maximizing an objective function. The plant can be considered as a reference-to-output map that has an extremum which is the operating point where the objective function is maximized. Three different ESC approaches are considered and compared in this study.

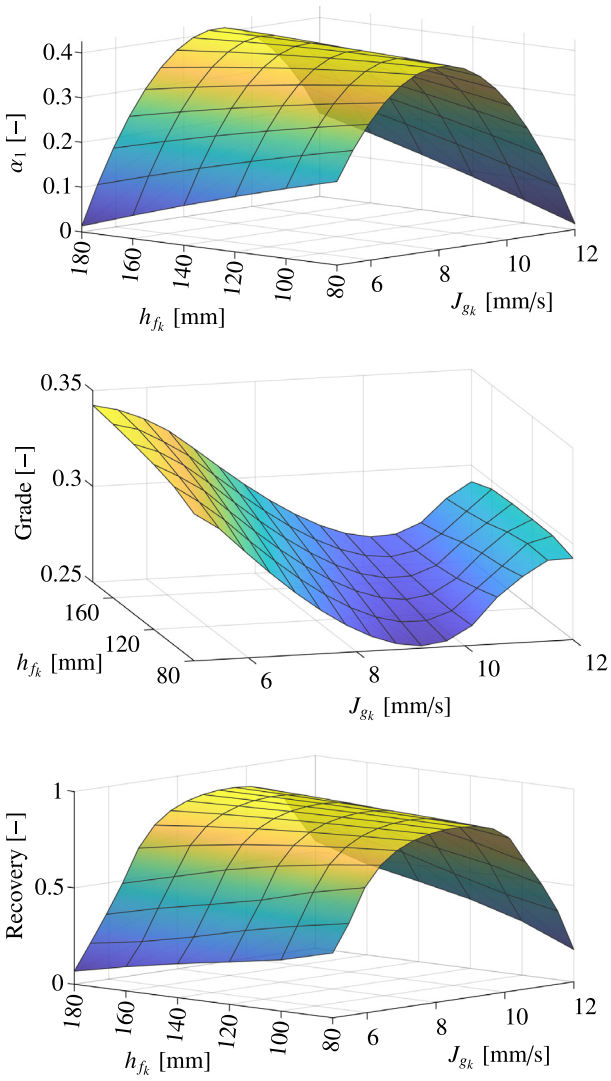

Fig. 2. 3D surface map of the steady-state model simulation showing the effect of the aeration rate and froth height on air recovery, grade and recovery, respectively. Only the air recovery for cell 1 is shown, but the shape is representative of all of the cells.

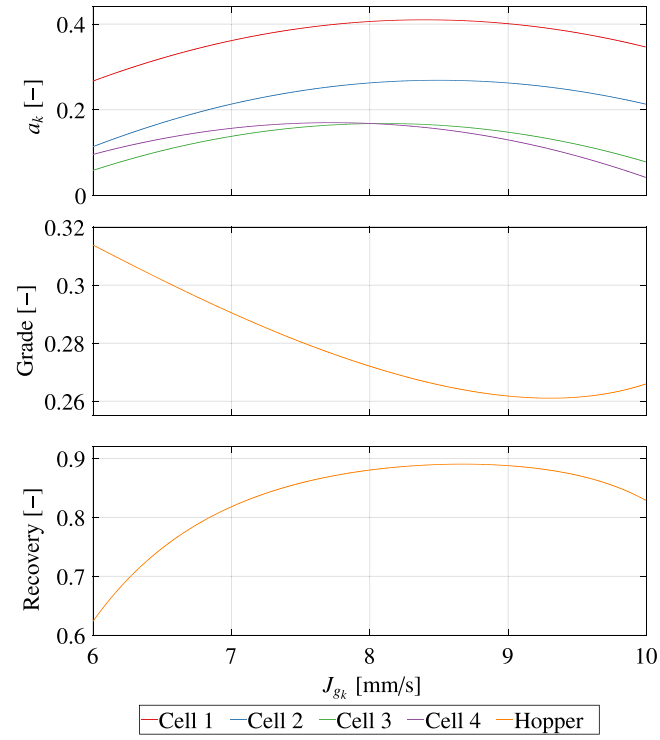

Fig. 3. Steady-state model simulation showing the effect of the aeration rate on air recovery, hopper grade and hopper mineral recovery, respectively, at a constant froth height.

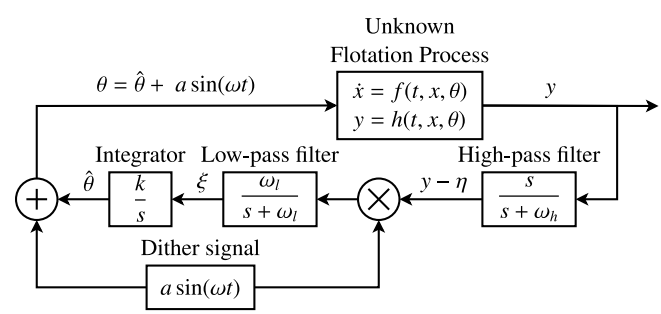

Fig. 4. Extremum seeking control scheme.
Source: Adapted from [12].

5.1. Perturbation-based extremum seeking control

When the reference-to-output map is unknown or contains uncertainty, it is necessary to use some sort of adaptation to find the extremum that maximizes the output [12]. A perturbation-based ESC (PESC) uses a slow periodic signal added to the input of the system to perturb the plant and steer the plant through the map towards the extremum. The controller adjusts the input based on the gradient extracted from the measured objective function as it changes due to the perturbations added to the input. The continuous perturbations allow the ESC to track an unknown time-varying optimum over time, even in the presence of external disturbances. One advantage of ESC is that the controller is model-free. Therefore, as long as the objective function has a maximum and is convex, the controller does not require any knowledge of the process to steer the process to the optimal operating point [19].

Fig. 4 shows the peak-seeking feedback scheme of a perturbation-based ESC. In the diagram, the flotation process is represented by the functions $\dot{x} = f(t, x, \theta)$ and $y = h(t, x, \theta)$. The process dynamics are unknown to the controller, and the functions f and h are considered as unknown black-box functions that take an input, θ, and provide an output, y, which is the measured objective function. The dither signal is a slow periodic perturbation, $a\sin(\omega t)$, where a is the amplitude, and ω is the perturbation frequency. The dither signal is added to $\hat{\theta}$, the best estimate of the optimal operating point (θ^*). The perturbations create a periodic response in the output, which the high-pass filter isolates by removing the steady-state component from y, resulting in the filtered output, $y - \eta$. The periodic response in the output will either be in or out of phase with the dither signal depending on the location of $\hat{\theta}$ relative to θ^*. The product of $y - \eta$ and the dither signal contains the gradient, ξ, which is extracted with the low-pass filter. The sign of the gradient, ξ, provides the direction to the integrator for moving $\hat{\theta}$ towards θ^*. The integrator gain, k, controls how aggressive the ESC will be and has to be selected sufficiently small to ensure convergence [12], but not too small as that would negatively affect the transient performance of the controller. The closed-loop system dynamics

of Fig. 4 are summarized as,

$$\dot{x} = f\left(t, x, \theta\right), \tag{20a}$$

$$y = h\left(t, x, \theta\right), \tag{20b}$$

$$\dot{\hat{\theta}} = k\xi, \tag{20c}$$

$$\dot{\xi} = -\omega_l \xi + \omega_l \left(y - \eta\right) a \sin\left(\omega t\right), \tag{20d}$$

$$\dot{\eta} = -\omega_h \eta + \omega_h y. \tag{20e}$$

For the ESC to operate effectively, the perturbation frequency has to be slow enough that the reference-to-output map of the plant appears as a static map. The static map ensures that the plant dynamics do not interfere with the ESC and that the controller can search along the static map for the optimum operating point. The system, therefore, has three time scales with sufficient separation between the scales. The fastest time scale is the process dynamics of the plant, together with the stabilizing and regulatory controllers. The next time scale is the periodic perturbations, which must be slower than the process dynamics. The filters in the ESC scheme are the slowest time scale, as the cut-off frequencies have to be lower than the frequency of the perturbation signal. The amplitude of the dither signal should be selected to be larger than the expected input noise and large enough that the plant response to the dither signal is detectable in the measurement noise of the objective function. However, since the measured objective function is representative of the performance of the plant, a too-large dither signal may reduce the performance of the plant.

5.2. Time-varying extremum seeking control

The time-varying ESC (TESC) is based on the estimation of the gradient as a time-varying parameter which removes the need for averaging the results and minimizes the impact of the dither signal choice by providing more freedom in tuning the ESC to improve the transient performance [20]. The controller first estimates the time-varying parameter, θ, the gradient of the static map, which is defined as,

$$\theta = \frac{\partial \ell}{\partial u}, \tag{21}$$

where ℓ is the static map and u is the time-varying input. y is the objective function to be maximized,

$$y(t) = \ell(u(t)). \tag{22}$$

This estimate of the gradient, $\hat{\theta}$, is then used in the controller to achieve the extremum seeking task. The estimation error is given by

$$e = y - \hat{y}. \tag{23}$$

The closed loop ESC system is shown in Fig. 5, and the system equations are,

$$\dot{x} = f\left(t, x, u\right), \tag{24a}$$

$$y = h\left(t, x, u\right), \tag{24b}$$

$$\dot{u} = -k\hat{\theta} + d, \tag{24c}$$

$$\dot{\hat{\theta}} = \text{Proj}\left(\Sigma^{-1}(c(e - \hat{\eta}) - \sigma\hat{\theta}), \hat{\theta}\right), \tag{24d}$$

$$\dot{\hat{\eta}} = -K\hat{\eta}, \tag{24e}$$

$$\dot{c} = -Kc + \dot{u}, \tag{24f}$$

$$\dot{\hat{y}} = \dot{u}^T\hat{\theta} + Ke + c^T\dot{\hat{\theta}}, \tag{24g}$$

$$\dot{\Sigma}^{-1} = -\Sigma^{-1}(cc^T)\Sigma_{-1} + k_T\Sigma^{-1} - 2\sigma\Sigma^{-2}, \tag{24h}$$

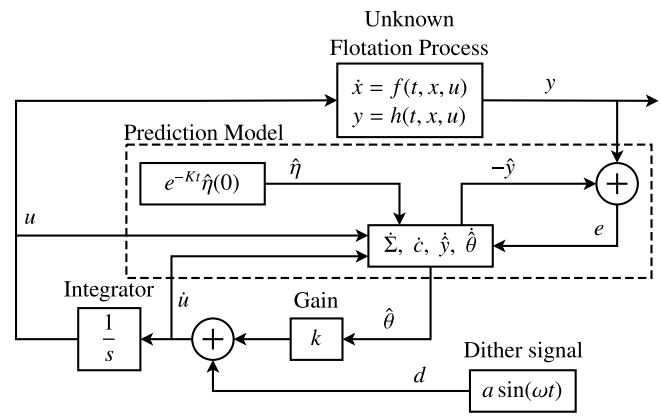

Fig. 5. Time-varying extremum seeking control scheme.
Source: Adapted from [13].

where K and k_T are estimation gains. K is defined as,

$$K = k_{\eta_1} + k_{\eta_2} c^T c. \tag{25}$$

The positive gains k_{η_1}, k_{η_2}, σ, k_T, k and the dither signal $d = a\sin(\omega t)$ are all tuning parameters that can be selected such that the ESC system converges to the optimization extremum of (22) [13]. The projection in (24d) is given by,

$$\dot{\hat{\theta}} = \begin{cases} \phi & \text{if } \mathcal{P}(\hat{\theta}) > 0 \text{ or } \nabla_{\hat{\theta}}\mathcal{P}(\hat{\theta})\phi \leq 0 \\ \left(I - \dfrac{\nabla_{\hat{\theta}}\mathcal{P}(\hat{\theta})^T \nabla_{\hat{\theta}}\mathcal{P}(\hat{\theta})}{\|\nabla_{\hat{\theta}}\mathcal{P}(\hat{\theta})\|^2}\right)\phi & \text{otherwise,} \end{cases} \tag{26}$$

where $\phi = \Sigma^{-1}\left(c(e - \hat{\eta}) - \sigma\hat{\theta}\right)$ and the function $\mathcal{P}(\hat{\theta})$ is defined as,

$$\mathcal{P}(\hat{\theta}) = \|\hat{\theta}\|^2 - z_\theta^2, \tag{27}$$

with its gradient,

$$\nabla_{\hat{\theta}}\mathcal{P}(\hat{\theta}) = 2\hat{\theta}^T. \tag{28}$$

The constraint, z_θ is the upper limit on the size of the norm of the gradient estimate, $\hat{\theta}$.

The diagram in Fig. 5 shows the TESC control scheme implemented on the flotation process with unknown dynamics. The dashed block is the prediction model given in (24d)–(24h). The optimization gain, k, controls the speed of the response, but an increase in k reduces the effect of the dither signal on u, which negatively affects the estimation routine. In general, there exists a maximum value of the gain k that can be achieved [20]. A small value for parameter σ ensures that Σ does not become too small which could impede the estimation routine. However, z_θ has to increase as σ becomes smaller.

5.3. Simplex extremum seeking control

The Simplex ESC (SESC) is based on the Nelder–Mead algorithm [21]. This method has limitations when used in time-varying conditions and in the presence of disturbances, but was selected because it is a simple heuristic controller with a fast convergence time that is easy to implement and tune. The algorithm works by creating a simplex of function values with $n + 1$ vertices, where n is the number of variables in the objective function. The simplex adapts to the static map and contracts to the extremum by replacing the lowest vertex with a new point for each iteration. Three operations are used to replace the

point - *reflection*, *contraction* and *expansion*. This iterative direct search method can efficiently find the extremum of the objective function without using any gradient information. The algorithm is shown in the flow diagram in Fig. 6. In the initialization step, a simplex is created around the initial input value. The simplex consists of $n+1$ vertices, labeled as $v_1, \ldots, v_n, v_{n+1}$, and the objective function is evaluated at each of the vertices to find the function values,

$$f(v_1), \ldots, f(v_n), f(v_{n+1}). \tag{29}$$

The next step is to order the vertices from best to worst. Since the aim of the simplex method is to minimize the objective function[1], the minimum function value (best point) will be $f(v_1)$, and the maximum function value (worst point) will be $f(v_{n+1})$. The simplex is then ordered to be,

$$f(v_1) \leq \cdots \leq f(v_n) \leq f(v_{n+1}). \tag{30}$$

The flow diagram in Fig. 6 is then followed, moving through the operations until a new point is accepted. The operation equations are given by,

$$v_r = \bar{v} + \alpha(\bar{v} - v_{n+1}), \qquad (\textit{reflection}) \tag{31a}$$

$$v_e = v_r + \gamma(v_r - \bar{v}), \qquad (\textit{expansion}) \tag{31b}$$

$$v_{co} = \bar{v} + \rho(v_r - \bar{v}), \qquad (\textit{outside contraction}) \tag{31c}$$

$$v_{ci} = \bar{v} + \rho(v_r - v_{n+1}), \qquad (\textit{inside contraction}) \tag{31d}$$

where $\bar{v}$ is the centroid of the simplex,

$$\bar{v} = \frac{\sum_{k=1}^{n} v_k}{n}. \tag{32}$$

The last operation is a *shrink* step where all the points in the simplex except for the best point are shrunk according to,

$$v_i = v_1 + \sigma(v_i - v_1), \quad i = 2, \ldots, n+1. \tag{33}$$

The coefficients used in the operations should satisfy,

$$\alpha > 0, \quad \gamma > 1, \quad \gamma > \alpha, \quad 0 < \rho < 1, \quad \text{and} \quad 0 < \sigma < 1. \tag{34}$$

When a non-shrink step occurs (reflect, expand, contact outside or contract inside), the worst vortex v_{n+1} is discarded and replaced by the new accepted point. When a shrinking step occurs, only the best point is kept, and the rest are all replaced. The new simplex is then sorted, and the process repeats with a new iteration.

When the simplex method is applied to a dynamic process, the function evaluations take place by assigning the calculated vertex value (v_r, v_e, v_{co} or v_{ci}) to the input of the process and allowing a sufficient time period (T_s) for the process to reach steady-state before measuring the output of the process and assigning it to the function value ($f(v_r), f(v_e), f(v_{co})$ or $f(v_{ci})$). To prevent undesired plant behavior, such as overshoot and aggressive plant responses due to large step sizes, a ramp function can be used to linearly interpolate the operating point between step changes [22]. The controller is set up to linearly ramp the process input value to the new vortex value in $T_s/2$ h and then keep the input constant for $T_s/2$ h.

The advantage of SESC is that the controller can make relatively large step changes and potentially reach the extremum quicker than, for example, the other two ESC approaches discussed previously. The controller evaluates the objective function itself and not the gradient. As a result, the method is much more resistant to noise and variations in the objective function. The size of the simplex decreases as the process approaches the extremum, resulting in increasingly smaller perturbations. However, this also means that the controller loses the ability to track a time-varying extremum. If the optimum changes after the controller converged to a point, the algorithm would not be able to adapt and track the new optimum unless the method is reinitialized with a new simplex so that the optimization can start again. The frequency of reinitialization needs to be selected carefully to prevent unnecessary disturbances or reduced tracking performance. An alternative solution is to limit the minimum simplex size to allow the method to continue to perturb the process and track any changes in the optimum [23].

[1] For the flotation circuit, the objective function will be the negative of the air recovery as the aim is to maximize air recovery.

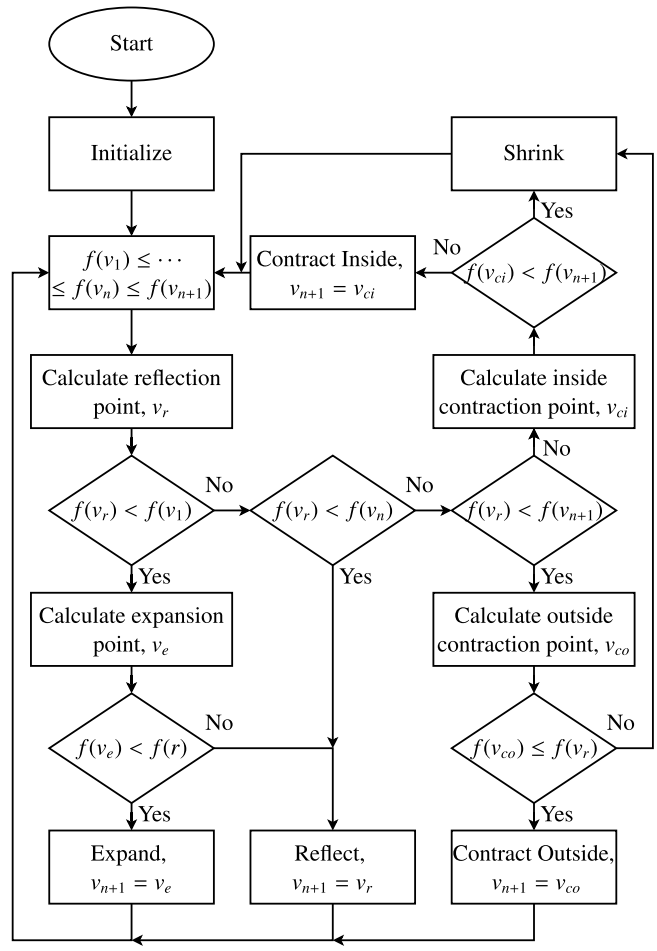

Fig. 6. Simplex extremum seeking control scheme flow diagram.

6. Simulations

The purpose of the simulations is to demonstrate how well each of the different ESCs works as an optimization controller on a flotation circuit and to compare the relative performances. Fig. 7 shows a diagram of the flotation cells and controllers implemented. Each of the four flotation cells has a cross-sectional area of 8.82 m^2 and a cell height of 1.4 m, and the nominal feed flow rate to the first cell is 730 m^3/h. The flotation cells are modeled with the dynamic flotation model given in Section 3. On the tailings stream of each of the cells, as well as the outflow of the hopper, PI-controllers are implemented to stabilize the pulp levels, L_k. The levels are controlled to a setpoint while the froth height of each cell, h_{f_k}, is kept constant. These regulatory controllers keep the cell levels and hopper level constant in the

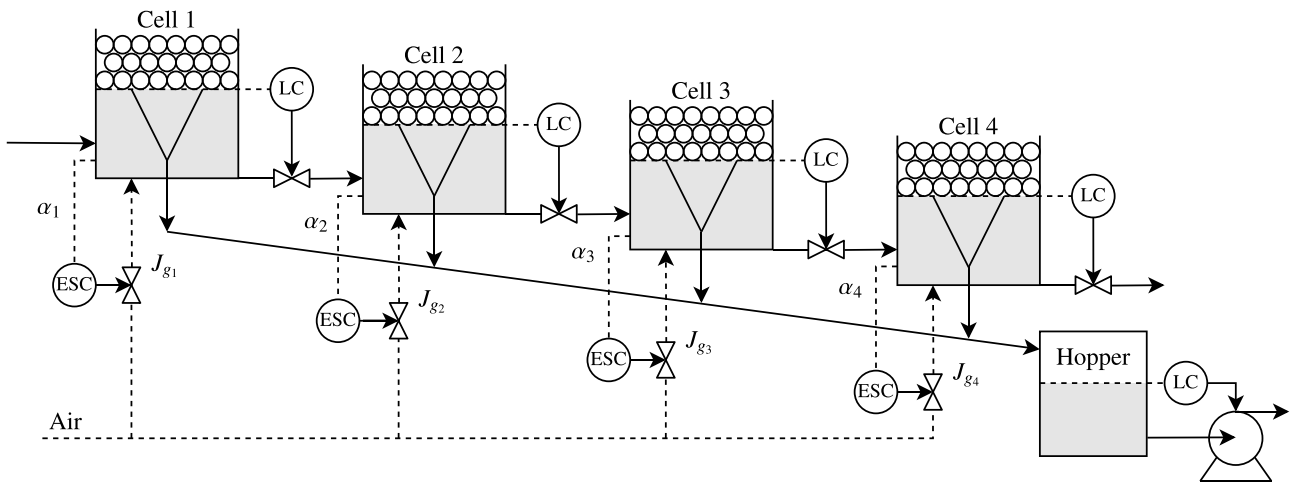

Fig. 7. The control architecture for the flotation circuit used in the simulation study.

presence of any disturbance in the plant. The regulatory controllers handle all the constraints of the flotation circuit and keep the plant operating within the allowed operating ranges. The ESC controllers do not include any constraints explicitly.

A separate ESC is implemented on each of the cells to maximize the air recovery, α_k, by manipulating the aeration rate to the cells. The local optimization problem of finding the aeration rate that produces the maximum air recovery can be solved in each of the cells independently of how the other cells are being operated.

The flotation plant model and the ESC controllers are simulated with a 4*th* order *Runge–Kutta* numerical integration method using a fixed time-step of 10 s. White Gaussian noise with a noise level of −50 dB is added to J_{g_k} and −30 dB is added to h_{f_k} as input noise. White Gaussian noise with a noise level of −50 dB is added to α_k and −50 dB is added to L_k and L_H to evaluate the performance of the controllers in the presence of measurement noise. Process noise is also added to the model parameters of the air recovery model to replicate operating conditions similar to what is found in industry. White Gaussian noise with a level of −33 dB is added to α_{OS_k} and noise with a level of −47 dB is added to $K_{\alpha_{J_{gk}}}$.

6.1. Controller tuning

The four ESC controllers on the four flotation cells are all tuned with the same tuning parameters which are given in Table 4. These parameters are not necessarily the optimal choices but have been tuned to find a good balance between the transient response and robustness and should therefore enable a fair comparison between the controllers.

The three frequency tuning parameters used in the PESC method (ω, ω_l, and ω_h), are dependent on the plant dynamics and should be selected to create the required time-scale separation between the plant, dither, and optimization. The response time of the air recovery in a flotation cell, when a J_{g_k} step occurs, has been measured to be less than 5 min and as low as 1.5 min under ideal conditions and no noise. To create the time-scale separation, the period of the dither signal is selected to be 5 min, giving a frequency of $\omega = 75$ rad/h. The high-pass cutoff frequency is selected to be slightly lower than the dither frequency so that the filter can isolate the periodic response, and the low-pass cutoff frequency is selected much lower to extract only the gradient, ξ. The dither amplitude, a, and the integration gain, k, are tuned together with trial and error until a good balance is achieved between the transient performance and robustness. For a smaller amplitude, a larger integration gain is required to achieve similar transient performance, and for a larger amplitude, the gain should be reduced to ensure robustness.

Table 4
ESC parameters.

Method	Tuning parameter	Description
PESC	$a = 0.05$	Dither amplitude
	$\omega = 75$ rad/h	Dither frequency
	$\omega_h = 72$ rad/h	High-pass cutoff frequency
	$\omega_l = 0.36$ rad/h	Low-pass cutoff frequency
	$k = 250$	Integrator gain
TESC	$a = 0.0008$	Dither amplitude
	$\omega = 75$ rad/h	Dither frequency
	$k_T = 0.02$	Estimation gain
	$k_{\eta_1} = 0.25$	Estimation gain constant
	$k_{\eta_2} = 0.25$	Estimation gain constant
	$k = 0.007$	Optimization gain
	$\sigma = 0.0001$	Positive constant
	$z_\theta = 1$	Uncertainty set radius
SESC	$\alpha = 0.65$	Reflection coefficient
	$\gamma = 2$	Expansion coefficient
	$\rho = 0.5$	Contraction coefficient
	$\sigma = 0.5$	Shrinking coefficient
	$T_s = 0.25$ h	Time to reach steady-state

For the TESC controller, the dither signal frequency and amplitude, and the optimization gain can be tuned similarly to the dither and integrator gain of the PESC controller. However, since the dither signal is added before the integrator, instead of after as in the PESC controller, a much smaller amplitude is required to produce a similar perturbation to the plant. The rest of the tuning parameters are less intuitive to select because the parameters are interconnected and dependent on each other and require some trial and error to find appropriate values. The estimation gain and estimation gain constants determine how aggressive the estimation of the time-varying parameter is. These parameters should be as large as possible to improve the transient response while keeping the controller stable and robust. The positive constant, σ, is selected to be small to improve the gradient estimation routine and z_θ is selected large enough to not constrain the gradient estimation.

The SESC controller is easy to tune, and the standard values for the coefficients as described in Nelder and Mead [21] ($\alpha = 1$, $\gamma = 2$, $\rho = 0.5$, and $\sigma = 0.5$) often lead to optimal performance. Only the reflection coefficient was reduced from the standard value to $\alpha = 0.65$ to make the controller less aggressive. The setting time parameter, T_s, should be selected based on the plant dynamics.

The time should be chosen as small as possible to improve the transient performance of the controller, but still large enough to allow the plant to reach a steady state before making the next control move. The parameter was selected to be $T_s = 15$ min which means that control input is adjusted linearly to a new value over 7.5 min and then kept constant for 7.5 min to allow enough time for the plant to reach steady state before the next control move takes place.

6.2. Simulation scenarios

Three simulation scenarios are considered:

1. The optimization ability of ESC ($t = 0$ h to $t = 120$ h).

In this scenario, only the ability of the ESC to find the optimum is evaluated. The simulation starts at a sub-optimal operating point, and the ESCs optimize the flotation circuit over a period of 5 days (120 h). During this time period, there are no external disturbances or changes to the process.

2. The disturbance rejection ability of ESC ($t = 120$ h to $t = 240$ h).

In this scenario, the ability of the ESC to reject disturbances is evaluated. Continuing from the previous scenario, at $t = 140$ h, the plant is subjected to a large disturbance that significantly changes the peak air recovery operating point. In reality, the disturbances in industrial plants are usually much smaller and more gradual. The disturbance was made by decreasing $K_{\alpha_{J_{gk}}}$ in (11) by 15% and decreasing α_{OS_k} by 5% over a 3 h period. Since the effect of individual specific disturbances such as changes in mineral grade and percentage solids are not modeled, the step-changes in $K_{\alpha_{J_{gk}}}$ and α_{OS_k} aim to simulate any combination of disturbances that influence the optimal peak air recovery operating point. These parameter changes cause the curves in Fig. 2 to shift, and the operating point essentially moves to a different place on the curve for which the controller needs to find the peak again.

3. The tracking ability of ESC ($t = 240$ h to $t = 360$ h).

In this scenario, the ability of the ESC controllers to track a time-varying optimum is evaluated. Starting at $t = 260$ h, the aeration rate that results in maximum air recovery, as well as the maximum air recovery value, are continuously varied until $t = 360$ h. A time-varying random walk is added to the parameters, $K_{\alpha_{J_{gk}}}$ and α_{OS_k}, which updates with a new random gradient every 5 h. The random gradients of the two parameters are determined by White Gaussian processes with magnitudes of -10 dB and -30 dB for the gradients of $K_{\alpha_{J_{gk}}}$ and α_{OS_k} respectively.

7. Results and discussion

7.1. The optimization ability of ESC ($t = 0$ h to $t = 120$ h).

The simulation results for the first 120 h are first shown separately for each of the three different controllers in Figs. 8–10 and then shown together on the same plot in Fig. 11. The top left plot is the air recovery (α_k) that has to be maximized, and below it, the aeration rate (J_{g_k}) plot shows the control inputs that the controllers use to steer the plant to that optimum. On the top right, the hopper grade (17) and mineral recovery (18) are plotted against time, and the middle plot shows the grade-recovery curve that can be used to evaluate the overall performance of the flotation plant quickly. Since the simulation allows the plant to reach steady-state over a long time period, the instantaneous recovery shown is not expected to differ significantly from the true recovery. The bottom plot is a projection of the air recovery on the 3D surface plot showing the effect of the entire range of input values. Since the froth height is controlled to a set point, the path that the controller takes will not vary much in the h_{f_k}−dimension. Fig. 12 also shows the projections of the air recovery, grade and recovery of all the controllers on the 3D surface plots from Fig. 2. The convergence time of the ESC controllers is measured as the time it takes the air recovery of all the cells to settle within 1% of the peak air recovery point. A 5 min moving average is used for the calculation to ensure that the noise does not affect the convergence time. The convergence times of the ESC controllers are summarized in Table 5. Figs. 11 and 12 show that the process starts at a sub-optimal operating point, and for the first 20 h the controllers are deactivated while the plant operates under regulatory level controllers only. At $t = 20$ h, the ESC controllers are activated and start to optimize the flotation plant by maximizing the air recovery. The PESC and TESC controllers, shown in Figs. 8 and 9 respectively, take very similar paths towards the peak air recovery point. The main difference is the speed of the convergence. As shown in Table 5, the TESC is able to react quicker than the PESC and is able to reach the peak air recovery more than 3 h faster than the PESC. The TESC controller is also more aggressive and noisy than the PESC controller and the aeration rate can be seen to vary much more around the optimal operating point. Once the peak air recovery is reached in each of the cells, the perturbations continue to keep the process at the optimal operating point.

The SESC controller, shown in Fig. 10, is quite different from the PESC and TESC controllers, resulting in a much more aggressive transient response due to larger step sizes. The ESC converges

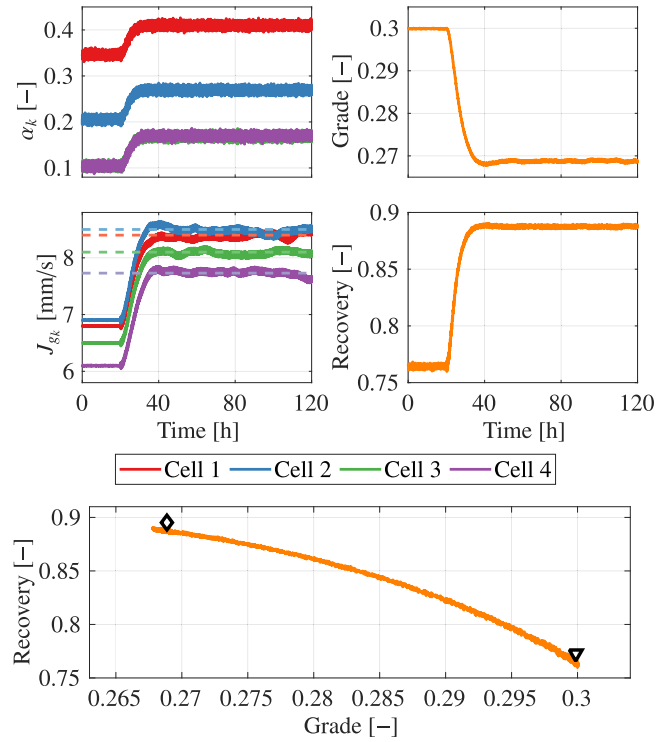

Fig. 8. PESC optimization simulation results. The dashed lines show the optimal aeration rates. The initial conditions are indicated by ▽ and ◇ is the final optimized operating point.

Table 5
Convergence time of the ESC controllers.

Controller	Convergence time
PESC	8.71 h
TESC	5.65 h
SESC	1.09 h

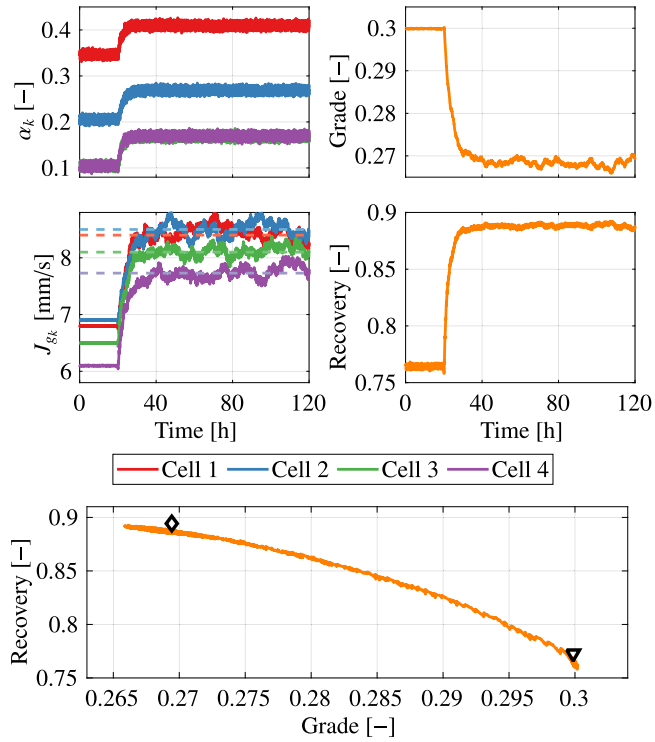

Fig. 9. TESC optimization simulation results. The dashed lines show the optimal aeration rates. The initial conditions are indicated by ▽, and ◇ is the final optimized operating point.

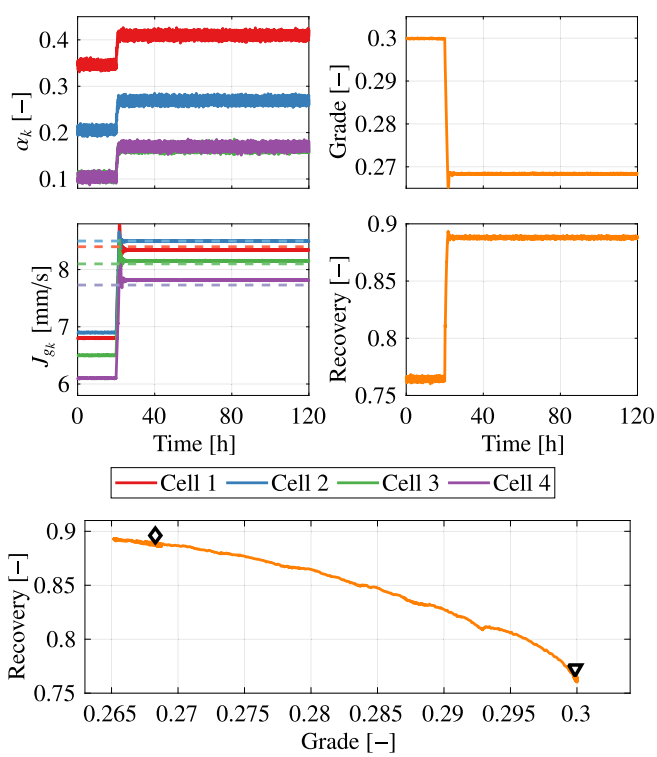

Fig. 10. SESC optimization simulation results. The dashed lines show the optimal aeration rates. The initial conditions are indicated by ▽, and ◇ is the final optimized operating point.

to the peak air recovery point more than 4.5 h faster than the TESC and more than 7.6 h faster than the PESC. As a result of

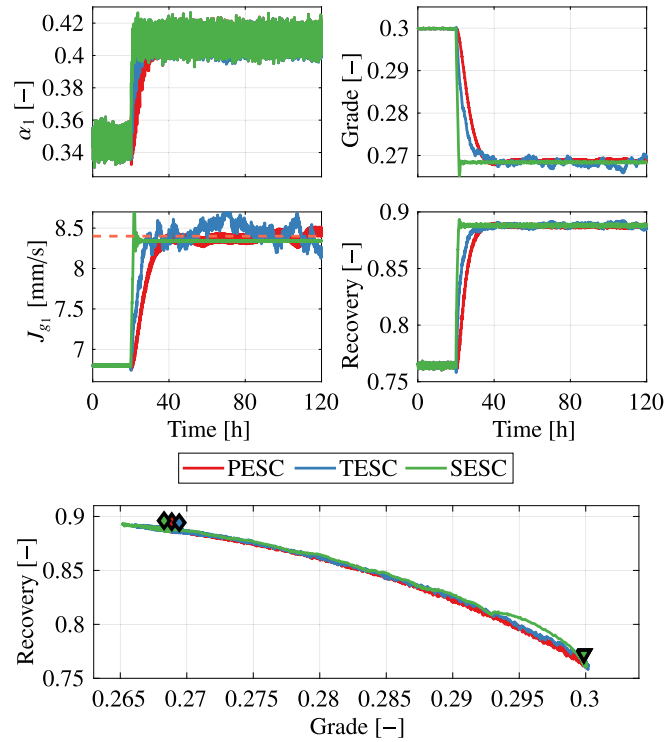

Fig. 11. Comparison of the optimization simulation results of PESC, TESC and SESC. The dashed line shows the optimal aeration rate. The initial conditions are indicated by ▽ and ◇ is the final optimized operating points. Only the air recovery and aeration rate for cell 1 are shown. The other cells have similar plots.

the relatively aggressive control action, the SESC controller can be seen to overshoot the optimal J_{g_k} operating point, and it also oscillates around the optimal point before settling. The larger step sizes of the SESC algorithm can be seen on the grade-recovery curve of Fig. 10, especially at the start of the optimization routine when the simplex is still relatively large. Since the simplex becomes increasingly smaller after the extremum has been reached, the SESC control input, J_{g_k}, has very small perturbations, if any, unlike the more noisy signals of the PESC and TESC controllers.

There is very little difference in the final optimized air recovery, hopper grade and recovery operating point where the controllers settle as all the ESCs are successful in finding the peak air recovery point. The ESCs increase the recovery up to 88.8% where it stabilizes close to the theoretical maximum mineral recovery of 89% as shown in Fig. 3. This increase in hopper mineral recovery comes at a cost of a reduced hopper grade which drops to below 26.9%. On the grade-recovery curves, the operating point moves from the bottom right at a high grade and low recovery towards the top left, where the recovery is maximized at a reduced grade. This relationship is also demonstrated in Fig. 12 where the grade is steered towards the valley while the recovery is being maximized.

7.2. The disturbance rejection ability of ESC (t = 120 h to t = 240 h).

The simulation results from the second 120 h are summarized in Fig. 13, showing how the different controllers react to the large disturbance simulated at $t = 140$ h. When the disturbance takes place, at $t = 140$ h in Fig. 13, operating conditions change, and the peak air recovery point is no longer at the same aeration rate as before, which causes the air recovery to drop to 35%. The PESC

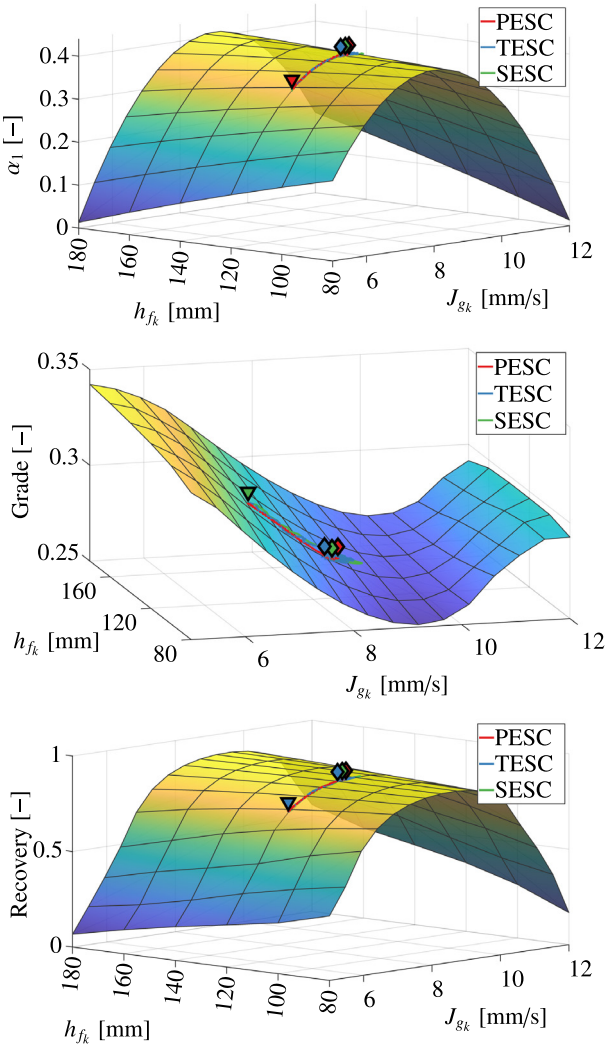

Fig. 12. Comparison of the optimization simulation results of PESC, TESC and SESC projected on the 3D surface maps. The initial conditions are indicated by ▽ and ◇ is the final optimized operating points. The data shown in this plot have been filtered to remove some of the noise and show the paths more clearly. Only the air recovery surface plot for cell 1 is shown. The other cells have similar surface plots.

and SESC controllers react to the disturbance by optimizing the air recovery again until the new peak air recovery operating point has been reached. The convergence times of the ESC controllers to reach the peak air recovery again after the disturbance are summarized in Table 6. The TESC controller is once again faster to react and reaches the optimum faster than the PESC controller. The ESC controllers decrease the aeration rate to steer the process to the peak air recovery operating point as the disturbance shifted the operating point to the other side of the parabola peak in Figs. 2 and 3. This is confirmed by the different shape of the grade-recovery curve in Fig. 13 and both the hopper grade and recovery that increases as the optimization continues. At the new peak air recovery operating point, the recovery is lower at 84.5%, but the grade is better at 28.9%. The theoretical maximum mineral recovery under these new operating conditions is 85%. The SESC controller cannot adjust to the disturbance because the simplex is already too small to provide a perturbation to steer the plant to the new optimum. Therefore, the SESC controller will keep operating at the sub-optimal operating point until the controller is reinitialized with a new simplex, and the optimization can start over.

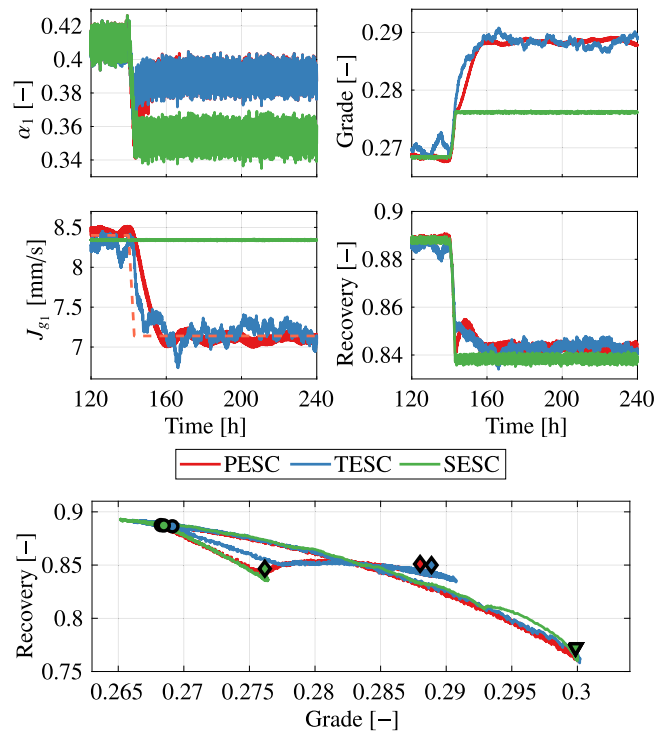

Fig. 13. Comparison of the optimization simulation results of PESC, TESC and SESC after the disturbance. The dashed line shows the optimal aeration rate. The initial conditions are indicated by ▽, ○ is when the disturbance takes place, and ◇ is the final optimized operating points. Only the air recovery and aeration rate for cell 1 are shown. The other cells have similar plots.

Table 6
Convergence time of the ESC controllers after the disturbance.

Controller	Convergence time
PESC	9.11 h
TESC	6.15 h
SESC	∞

7.3. The tracking ability of ESC ($t = 240$ h to $t = 360$ h).

The simulation results from the third 120 h are shown in Figs. 14–16, showing how well the different controllers can track a time-varying optimum which starts at $t = 260$ h. Both the gradient-based ESC controllers, PESC and TESC can track the optimal aeration rate as it changes. The SESC does not have the ability to track the time-varying optimum and the controller does not react to the changes. Even if the controller is reinitialized, it would only find the optimum once and then keep that operating point until the next re-initialization. The tracking performance of the TESC controller, shown in Fig. 15, is superior to the tracking performance of the PESC controller. This algorithm is ideally suited to tracking the changes in the optimal aeration rate and the system is kept close to the peak air recovery at all times. The PESC also track the changes sufficiently well in the long term, however, the controller is slower to respond to sudden changes which can result in reduced performance.

7.4. Comparison

Comparing the three ESCs, each has some clear advantages and disadvantages. All the controllers are successful in optimizing the flotation circuit from a sub-optimal operating point to the peak

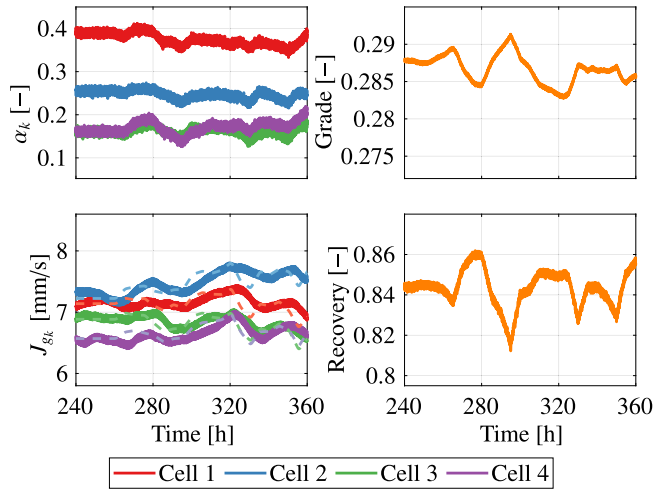

Fig. 14. PESC tracking simulation results. The dashed lines show the optimal aeration rates.

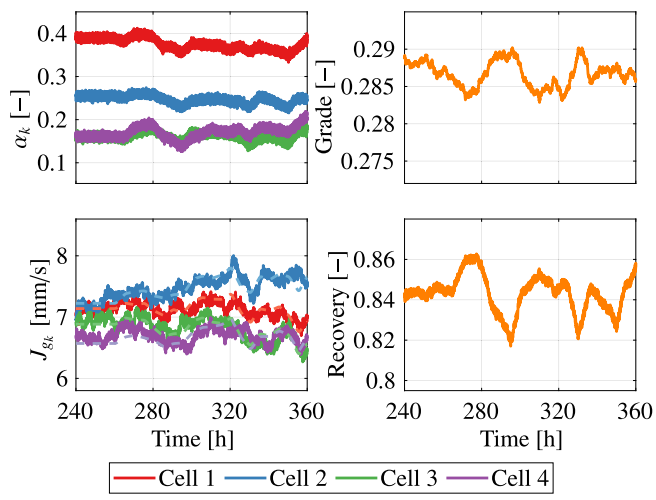

Fig. 15. TESC tracking simulation results. The dashed lines show the optimal aeration rates.

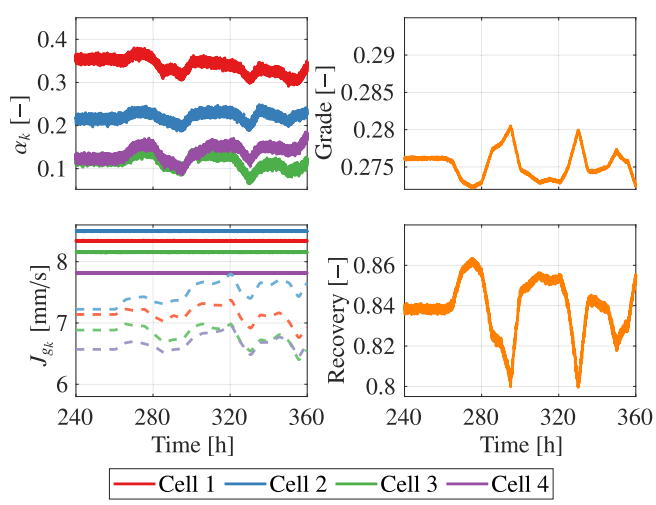

Fig. 16. SESC tracking simulation results. The dashed lines show the optimal aeration rates.

Table 7
Comparison of convergence times of the ESC controllers.

Controller	Convergence time	
	Optimization	Disturbance rejection
PESC	8.71 h	9.11 h
TESC	5.65 h	6.15 h
SESC	1.09 h	∞

air recovery operating point by adjusting only the aeration rate. The PESC is simple to tune, but the performance can be limited by the choice of dither signal and the dynamics of the plant.

The TESC provides more freedom to tune the controller to improve the performance beyond the choice of dither signal. However, the many tuning parameters can be difficult to tune well. The TESC can also perform well with a smaller dither signal than the PESC, i.e., in this example, the chosen TESC dither amplitude is much smaller than the PESC dither amplitude (Table 4). The convergence times of the different controllers are summarized in Table 7. SESC has the fastest convergence time and is also dither-free with no perturbations visible in the output that can reduce the plant performance at the optimum. The SESC controller can tolerate higher noise levels because of the lack of dependence on gradient information. The SESC controller is unsuitable for tracking a time-varying extremum due to changes in the operating conditions. An operator will need to reinitialize the SESC to track a new extremum when they are aware of significant changes in the operating conditions.

Both the PESC and TESC controllers are capable of tracking a time-varying extremum and the controllers will keep the plant operating at the optimal operating point continuously. TESC has superior tracking performance and can efficiently track relatively fast changes in the extremum. A big advantage of all the controllers is that they are not dependent on a plant model to optimize the process. The ESCs can operate effectively with only basic knowledge of the response time and dynamics of the plant.

8. Conclusion

This paper demonstrates in simulation that the three different ESCs investigated are all able to manipulate the aeration rate of a flotation circuit to maximize air recovery. The ESCs move the flotation circuit from a suboptimal operating point to the peak air recovery operating point. The gradient-based PESC and TESC are successful in continuously tracking the optimum, and after a simulated disturbance, the ESCs can adapt to the time-varying extremum and once again reaches the new peak air recovery operating point. The SESC is able to optimize to the extremum relatively quickly but then maintains the same operating point and does not adapt after the introduction of the disturbance or changes in the plant conditions. The SESC must be reinitialized when the operating conditions change to keep tracking the optimum.

In summary, when comparing the ESC controllers, PESC is simple to tune but is quite slow, and the performance can be limited by the choice of dither signal and the dynamics of the plant. TESC provides more freedom for tuning to improve the transient performance and can use a smaller dither signal but can be more challenging to tune well. SESC is easy to tune, has the fastest convergence time and is dither free, but is not suitable to track a constantly varying extremum.

The ESCs take a relatively long time to converge to an optimum. If the peak air recovery operating point changes quickly because of a large disturbance, it is difficult to effectively track the changing optimum. Phillpotts et al. [10] suggest that a controller with a convergence time of 3 h is sufficient to track a time-varying optimum. This is possible with the SESC controller, even if

the current operating point is relatively far from the optimum. If the other two controllers start close to the optimum, they should also be able to track a change in the optimum for relatively slow disturbances.

The ESC controllers are model-free and do not need a plant model to optimize the plant. This is an important advantage since flotation models are often very complicated and difficult to fit to industrial data. Air recovery measurements can sometimes be unreliable and can cause the ESCs to operate the flotation circuit at a different point from where true peak air recovery occurs, resulting in sub-optimally performance. However, Phillpotts et al. [10] demonstrated that air recovery measurements can successfully be used for control.

The measurement noise in industrial plants, especially in the measurement of air recovery using vision systems, can reduce the performance of the ESC controllers. For very noisy environments, the perturbation amplitude may need to be increased for the change in air recovery to be visible amid the noise. As long as a change is visible, the controller will be able to move the process to a more optimal operating point. Air recovery measurements will continue to improve as froth image analysis technology advances [24].

In future work, the convergence time of the ESC controller can potentially be improved by setting up a fast air recovery control loop that manipulates the aeration rate. The ESC controller can then be used to manipulate the setpoint of this loop. Alternatively, the SESC controller can be combined with either the PESC or TESC controller to form a hybrid controller to benefit from the advantages of both controllers. The hybrid controller will first use the SESC to find the initial optimum and then switch over to either PESC or TESC to track the optimum. The controller can switch back to a reinitialized SESC when a large disturbance or operating change is observed. The advantages of the SESC and PESC controllers are that they are relatively simple for an operator to understand and maintain for implementation on an industrial plant.

Declaration of competing interest

The authors declare that they have no known competing financial interests or personal relationships that could have appeared to influence the work reported in this paper.

Data availability

No data was used for the research described in the article.

Acknowledgments

This work is based on research supported in part by the National Research Foundation of South Africa (Grant numbers 130380 & 132380).

References

[1] I. Jovanović, I. Miljanović, Contemporary advanced control techniques for flotation plants with mechanical flotation cells - A review, Miner. Eng. 70 (2015) 228–249, http://dx.doi.org/10.1016/j.mineng.2014.09.022.

[2] H. Laurila, J. Karesvuori, O. Tiili, Strategies for instrumentation and control of flotation circuits, Miner. Process. Plant Des. Pract. Control 2 (2002) 2174–2195.

[3] I.K. Craig, I. Koch, Experimental design for the economic performance evaluation of industrial controllers, Control Eng. Pract. 11 (2003) 57–66.

[4] P. Quintanilla, S.J. Neethling, D. Navia, P.R. Brito-Parada, A dynamic flotation model for predictive control incorporating froth physics. Part I: Model development, Miner. Eng. 173 (2021) 107192, http://dx.doi.org/10.1016/j.mineng.2021.107192.

[5] B.J. Shean, J.J. Cilliers, A review of froth flotation control, Int. J. Miner. Process. 100 (3–4) (2011) 57–71, http://dx.doi.org/10.1016/j.minpro.2011.05.002.

[6] L.G. Bergh, J.B. Yianatos, The long way toward multivariate predictive control of flotation processes, J. Process Control 21 (2) (2011) 226–234, http://dx.doi.org/10.1016/j.jprocont.2010.11.001.

[7] C.D. Smith, K. Hadler, J.J. Cilliers, Flotation bank air addition and distribution for optimal performance, Miner. Eng. 23 (11–13) (2010) 1023–1029, http://dx.doi.org/10.1016/j.mineng.2010.05.003.

[8] K. Hadler, J.J. Cilliers, The relationship between the peak in air recovery and flotation bank performance, Miner. Eng. 22 (5) (2009) 451–455, http://dx.doi.org/10.1016/j.mineng.2008.12.004.

[9] K. Hadler, C.D. Smith, J.J. Cilliers, Recovery vs. mass pull: The link to air recovery, Miner. Eng. 23 (11–13) (2010) 994–1002, http://dx.doi.org/10.1016/j.mineng.2010.04.007.

[10] D. Phillpotts, B. Whitehead, S. Ramatsoma, Monitoring of air recovery for froth flotation optimisation on an industrial circuit, in: XXII International Mineral Processing Congress, Cape Town, South Africa, 2020, pp. 3348–3357.

[11] D.A. Wepener, J.D. le Roux, I.K. Craig, Disturbance propagation through a grinding-flotation circuit, IFAC-PapersOnLine 54 (21) (2021) 19–24, http://dx.doi.org/10.1016/j.ifacol.2021.12.004.

[12] M. Krstić, H.H. Wang, Stability of extremum seeking feedback for general nonlinear dynamic systems, Automatica 36 (4) (2000) 595–601, http://dx.doi.org/10.1016/S0005-1098(99)00183-1.

[13] M. Guay, E. Moshksar, D. Dochain, A constrained extremum-seeking control approach, Internat. J. Robust Nonlinear Control 25 (16) (2015) 3132–3153, http://dx.doi.org/10.1002/rnc.3254.

[14] M. Benosman, Learning-Based Adaptive Control: An Extremum Seeking Approach – Theory and Applications, first ed., Butterworth-Heinemann, Oxford, 2016, p. 275(12), http://dx.doi.org/10.1016/C2014-0-03287-X.

[15] D.A. Wepener, J.D. le Roux, I.K. Craig, Extremum seeking control of a flotation circuit using peak air recovery, IFAC PapersOnLine 55 (21) (2022) 61–66, http://dx.doi.org/10.1016/j.ifacol.2022.09.244.

[16] D.J. Oosthuizen, J.D. le Roux, I.K. Craig, A dynamic flotation model to infer process characteristics from online measurements, Miner. Eng. 167 (2021) 106878, http://dx.doi.org/10.1016/j.mineng.2021.106878.

[17] S.L. Jämsä-Jounela, M. Dietrich, K. Halmevaara, O. Tiili, Control of pulp levels in flotation cells, Control Eng. Pract. 11 (1) (2003) 73–81, http://dx.doi.org/10.1016/S0967-0661(02)00142-9.

[18] B. Shean, K. Hadler, J.J. Cilliers, A flotation control system to optimise performance using peak air recovery, Chem. Eng. Res. Des. 117 (2017) 57–65, http://dx.doi.org/10.1016/j.cherd.2016.10.021.

[19] H.-H. Wang, M. Krstić, G. Bastin, Optimizing bioreactors by extremum seeking, Internat. J. Adapt. Control Signal Process. 13 (8) (1999) 651–669.

[20] M. Guay, D. Dochain, A time-varying extremum-seeking control approach, Automatica 51 (2015) 356–363, http://dx.doi.org/10.1016/j.automatica.2014.10.078.

[21] J.A. Nelder, R. Mead, A simplex method for function minimization, Comput. J. 7 (4) (1965) 308–313.

[22] L. Ziolkowski, J.D. le Roux, I.K. Craig, Extremum seeking control for optimization of an open-loop grinding mill using grind curves, J. Process Control 114 (2022) 54–70, http://dx.doi.org/10.1016/j.jprocont.2022.04.005.

[23] Q. Xiong, A. Jutan, Continuous optimization using a dynamic simplex method, Chem. Eng. Sci. 58 (16) (2003) 3817–3828, http://dx.doi.org/10.1016/S0009-2509(03)00236-7.

[24] C. Aldrich, E. Avelar, X. Liu, Recent advances in flotation froth image analysis, Miner. Eng. 188 (2022) 107823, http://dx.doi.org/10.1016/j.mineng.2022.107823.